The Journal of Physiology

Changes in skeletal muscle and tendon structure and function following genetic inactivation of myostatin in rats

Christopher L. Mendias[1,2], Evan B. Lynch[1,2], Jonathan P. Gumucio[1,2], Michael D. Flood[1], Danielle S. Rittman[1], Douglas W. Van Pelt[3], Stuart M. Roche[1] and Carol S. Davis[2]

[1] *Department of Orthopaedic Surgery, University of Michigan, Ann Arbor, MI, USA*
[2] *Department of Molecular and Integrative Physiology, University of Michigan, Ann Arbor, MI, USA*
[3] *Department of Movement Science, University of Michigan, Ann Arbor, MI, USA*

Key points

- Myostatin is an important regulator of muscle mass and a potential therapeutic target for the treatment of diseases and injuries that result in muscle atrophy.
- Targeted genetic mutations of myostatin have been generated in mice, and spontaneous loss-of-function mutations have been reported in several species. The impact of myostatin deficiency on the structure and function of muscles has been well described for mice, but not for other species.
- We report the creation of a genetic model of myostatin deficiency in rats using zinc finger nuclease technology.
- The main findings of the study are that genetic inactivation of myostatin in rats results in increases in muscle mass without a deleterious impact on the specific force production and tendon mechanical properties. The increases in mass occur through a combination of fibre hypertrophy, hyperplasia and activation of the insulin-like growth factor-1 pathway, with no substantial changes in atrophy-related pathways.
- This large rodent model has enabled us to identify that the chronic loss of myostatin is void of the negative consequences to muscle fibres and extracellular matrix observed in mouse models. Furthermore, the greatest impact of myostatin in the regulation of muscle mass may not be to induce atrophy directly, but rather to block hypertrophy signalling.

Abstract Myostatin is a negative regulator of skeletal muscle and tendon mass. Myostatin deficiency has been well studied in mice, but limited data are available on how myostatin regulates the structure and function of muscles and tendons of larger animals. We hypothesized that, in comparison to wild-type ($MSTN^{+/+}$) rats, rats in which zinc finger nucleases were used to genetically inactivate myostatin ($MSTN^{\Delta/\Delta}$) would exhibit an increase in muscle mass and total force production, a reduction in specific force, an accumulation of type II fibres and a decrease and stiffening of connective tissue. Overall, the muscle and tendon phenotype of myostatin-deficient rats was markedly different from that of myostatin-deficient mice, which have impaired contractility and pathological changes to fibres and their extracellular matrix. Extensor digitorum longus and soleus muscles of $MSTN^{\Delta/\Delta}$ rats demonstrated 20–33% increases in mass, 35–45% increases in fibre number, 20–57% increases in isometric force and no differences in specific force. The insulin-like growth factor-1 pathway was activated to a greater extent in $MSTN^{\Delta/\Delta}$ muscles, but no substantial differences in atrophy-related genes were observed. Tendons of $MSTN^{\Delta/\Delta}$ rats had a 20% reduction in peak strain, with no differences in mass, peak stress or stiffness. The general morphology and gene expression patterns were similar between tendons of both genotypes. This large rodent model of myostatin deficiency did not have the negative consequences to muscle fibres and extracellular matrix observed in mouse models, and suggests that the greatest impact

 DOI: 10.1113/jphysiol.2014.287144

of myostatin in the regulation of muscle mass may not be to induce atrophy directly, but rather to block hypertrophy signalling.

(Received 12 November 2014; accepted after revision 23 January 2015; first published online 25 February 2015)
Corresponding author C. L. Mendias: Department of Orthopaedic Surgery, University of Michigan Medical School, 109 Zina Pitcher Place, BSRB 2017, Ann Arbor, MI 48109-2200, USA. Email: cmendias@umich.edu

Abbreviations CSA, cross-sectional area; ECM, extracellular matrix; EDL, extensor digitorum longus; F_o, maximal fibre isometric force; IGF-1, insulin-like growth factor-1; L_f, fibre length; L_o, length that results in maximal twitch force; miRNA, microRNA; $MSTN^{+/+}$, wild-type control; $MSTN^{\Delta/\Delta}$, myostatin knock-out; PCSA, physiological cross-sectional area; P_o, maximal isometric force; P_t, maximal twitch force; sF_o, specific force of fibre; sP_o, maximal isometric force normalized to muscle cross-sectional area; TA, tibialis anterior.

Introduction

Myostatin (GDF-8) is a member of the transforming growth factor-β superfamily of cytokines and a negative regulator of muscle mass. Myostatin binds to the activin type IIB (ACVR2B) and type IB (ACVRB) receptors and activates the Smad2/3, p38 MAPK and Erk1/2 signal transduction pathways (Gumucio & Mendias, 2012). Mice that are deficient in myostatin have an up to twofold increase in muscle mass, and administration of recombinant myostatin leads to profound atrophy and cachexia (McPherron *et al.* 2006; Zimmers *et al.* 2002). Myostatin also regulates the fibre-type composition of skeletal muscles, with myostatin-deficient mice demonstrating an increase in the accumulation and size of type II muscle fibres compared with control animals (Gentry *et al.* 2011). The lack of myostatin results in no change or an increase in production of maximal isometric force (P_o), and for some muscles there is also a decrease in specific force (sP_o), which is P_o normalized to muscle cross-sectional area (CSA) (Mendias *et al.* 2006, 2011; Gentry *et al.* 2011; Qaisar *et al.* 2012). As well as controlling muscle fibre size, type and contractility, myostatin also regulates the composition of the muscle and tendon extracellular matrix (ECM), in part by directly inducing the expression of type I collagen (Li *et al.* 2008; Mendias *et al.* 2008). While the targeted inhibition of myostatin has the potential to prevent muscle atrophy and fibrosis in degenerative diseases and injuries, the negative effects on force production and ECM stiffening observed in mouse models of myostatin deficiency have provided some pause in the potential therapeutic use of myostatin inhibitors.

In addition to mice, several animal models of myostatin deficiency have been described in the literature, including cattle, sheep, dogs, pigs and trout, as well as humans (Stinckens *et al.* 2011). While all organisms with deficiencies of myostatin display gross skeletal muscle hypertrophy, other than a common observation of increased muscle mass and limited data on fibre-type changes, there have been no detailed analyses of the impact of myostatin deficiency on the structure, mechanics and biochemistry of muscles from organisms other than mice. Recent advances in the ability to manipulate the rat genome using zinc finger technology have allowed for the inactivation of specific genes in the genome of rats (Geurts *et al.* 2009). Rats are 10–20 times larger than mice, and the skeletal muscle architecture, fibre-type composition and contractile function more closely resembles human muscle than mouse muscle (Eng *et al.* 2008). As the rat offers several advantages over mouse models, both for improving our understanding of basic muscle physiology and in the design of new therapies for muscle diseases, our objective was to evaluate the impact of myostatin deficiency on the contractile function, muscle architecture and fibre-type composition of skeletal muscles from rats with a targeted inactivation of their myostatin gene. We hypothesized that, compared with wild-type control ($MSTN^{+/+}$) rats, rats with a targeted knock-out of myostatin ($MSTN^{\Delta/\Delta}$) would exhibit an increase in muscle mass and total force production, a reduction in specific force production, an increased accumulation of type II muscle fibres, a decrease in connective tissue content and a stiffening of tendons.

Methods

Animals

This study was approved by the University of Michigan institutional animal care and use committee (protocol number PRO00003566). Animal handling and care was performed in accordance with US Public Health Service Policy on Humane Care and Use of Laboratory Animals and in agreement with the UK Home Office standards on research and testing using animals.

Myostatin-deficient rats ($MSTN^{\Delta/\Delta}$; strain SS-$Mstn^{em1}$) were generated at the Medical College of Wisconsin using zinc finger nuclease genome editing techniques as described by Geurts *et al.* (2009). Zinc finger nucleases engineered to target the sequence CTTATTCCTT-TGCAGCTGActttctAATGCAAGCGGATGGA were injected into SS/JrHsdMcwi rat embryos, which resulted in a deletion of a 16 bp region of DNA that contains the splice acceptor of exon 2 of myostatin (Fig. 1*A*). As the

propeptide of myostatin is required for the proper folding and assembly of the active myostatin peptide (Lee, 2004) and both exons encode regions of the propeptide that directly bind and stabilize myostatin (Jiang *et al.* 2004), the frameshift mutation caused by deleting the splice acceptor of exon 2 was predicted to disrupt the production of functional myostatin protein. Rats were backcrossed for several generations to ensure stable germline transmission of the mutant allele. Age-matched, wild-type rats from the SS/JrHsdMcwi strain ($MSTN^{+/+}$) were used as control animals.

The animals were housed in ventilated micro-isolator cages in specific pathogen-free conditions and provided with water and a standard Lab Diet 5001 chow (Purina Lab Diet, St Louis, MO, USA) *ad libidum*. Pups were weaned 3 weeks after birth, genomic DNA was obtained from tail biopsies, and *MSTN* genotype was determined using end-point PCR with primers (forward 5′-GGTGATTTTCTTCGTGTTTC-3′ and reverse 5′-AACATTTGGGCTTTCCAT-3′) that flank the targeted region of exon 2, resulting in a 102 bp amplicon for the $MSTN^{+}$ allele and 86 bp for the $MSTN^{\Delta}$ allele. Male homozygous wild-type ($MSTN^{+/+}$; $n = 6$) and homozygous myostatin-deficient ($MSTN^{\Delta/\Delta}$; $n = 7$) rats were used in this study (Fig. 1*B*).

Rats were shipped to the University of Michigan at 6 weeks of age, and their growth was monitored until use in experiments. At 24 weeks of age, rats were placed into deep anaesthesia using sodium pentobarbital (Vortex Pharmaceuticals, Dearborn, MI, USA) at a dose of 40 mg/kg via intraperitoneal injection, and tissues were removed for analysis. Left extensor digitorum longus (EDL) and soleus muscles were finely minced and used for biochemical measurements. Right EDL and soleus muscles

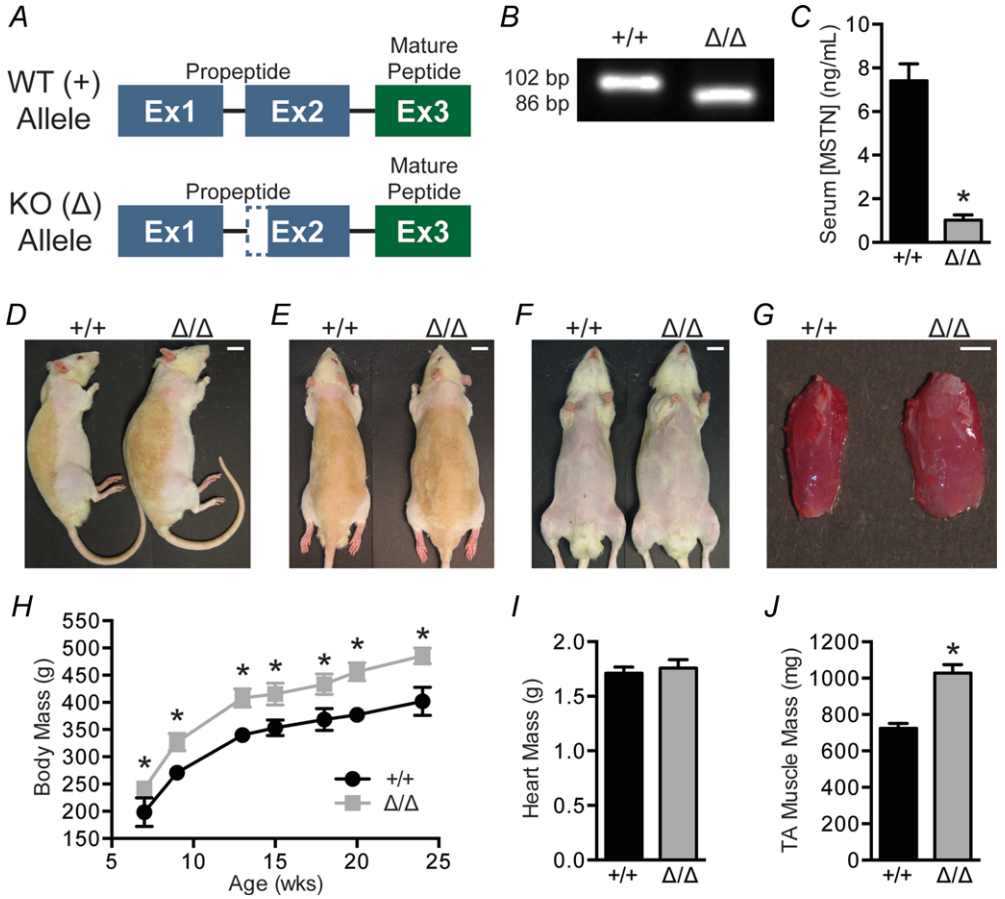

Figure 1. Genetic targeting approach and gross appearance of wild-type control (WT; $MSTN^{+/+}$) and myostatin knock-out (KO; $MSTN^{\Delta/\Delta}$) rats
A, diagram demonstrating the strategy used to target and inactivate myostatin by deleting a portion of exon 2 of myostatin that included the splice acceptor region. *B*, end-point PCR analysis using primers that flank the splice acceptor of exon 2, demonstrating effective deletion of a 16 bp region of this gene. *C*, concentration of myostatin (MSTN) in serum. *D–F*, gross appearance of 24-week-old $MSTN^{+/+}$ and $MSTN^{\Delta/\Delta}$ rats (scale bars represent 2 cm). *G*, gross appearance of tibialis anterior muscles (scale bar represents 0.5 cm). Growth curves (*H*), heart mass (*I*) and tibialis anterior (TA) muscle mass (*J*). In this and all subsequent figures, values are means ± SD; $n = 6$ for $MSTN^{+/+}$ rats and $n = 7$ for $MSTN^{\Delta/\Delta}$ rats. In this and all subsequent figures, differences were tested with Student's unpaired *t* tests; $^{*}P < 0.05$ different from $MSTN^{+/+}$ rats.

were used for whole-muscle contractility measurements and subsequent histology, and right tibialis anterior (TA) muscles were used for measurements of the contractility of single muscle fibres. The left plantaris tendons were used for mechanical properties measurements, while the right side was used for histology. After muscles were removed, 1–2 ml of blood was obtained from the left ventricle, and animals were killed by overdose of sodium pentobarbital (100 mg/kg, intraperitoneal) followed by removal of the heart.

Measurement of serum myostatin levels

Blood that was removed from rats was allowed to coagulate for 30 min, spun down at ∼1000*g* for 10 min, and serum was removed and stored at −80°C until use. Myostatin levels were measured in duplicate using an enzyme-linked immunosorbent assay kit (R&D Systems, Minneapolis, MN, USA), following the manufacturer's instructions. Before conducting the assay, serum samples were treated with 1 M HCl to release myostatin bound to the propeptide or other carrier proteins, followed by neutralization in 1.2 M NaOH–0.5 M Hepes. Absorbance values were read in a SpectraMax microplate reader (Molecular Devices, Sunnyvale, CA, USA).

Gene expression

Gene expression was performed as previously described (Gumucio *et al.* 2014; Mendias *et al.* 2012). Total RNA was isolated from EDL muscles, soleus muscles and plantaris tendons using an miRNeasy kit (Qiagen, Valencia, CA, USA) and treated with DNase I (Qiagen). The RNA integrity was confirmed using a Bioanalyzer RNA system (Agilent, Santa Clara, CA, USA). Using an RT^2 First Strand mRNA or microRNA (miRNA) kit (Qiagen), RNA was reverse transcribed and subsequently amplified in a CFX96 real-time thermal cycler (BioRad, Hercules, CA, USA) using RT^2 SYBR green-based qPCR reagents (Qiagen) and primers for specific mRNA or miRNA species. Most primers were purchased from Qiagen, with the exception of *IGF1Ea* and *IGF1Eb* (Heinemeier *et al.* 2007). Expression of target muscle mRNAs, tendon mRNAs and muscle miRNAs were normalized to the expression of the housekeeping transcripts β-actin, β2-microglobulin and *Rnu6*, respectively, and then further normalized to the expression of the $MSTN^{+/+}$ group (Schmittgen & Livak, 2008).

Akt/mTOR multiplex analysis

A Luminex-based system was used to measure total and phosphorylated proteins as previously described (Sharma *et al.* 2012; Castorena *et al.* 2014). Briefly, muscles were finely minced and placed in ice-cold Tissue Protein Extraction Reagent (Thermo Scientific, Rockford, IL, USA) supplemented with a protease and phosphatase inhibitor cocktail (Thermo Scientific), homogenized with a TissueRuptor (Qiagen) and vortexed for 10 min at 4°C. Samples were then spun at 12,000*g* for 10 min, and the supernatant was collected and stored at −80°C until use. Total protein content was determined using a BCA protein assay (Thermo Scientific), and 50 μg of total protein was analysed using Milliplex-MAP 11-plex Akt/mTOR total protein and phosphoprotein magnetic bead assays (EMD Millipore Corporation, Billerica, MA, USA). These assays measure the abundance of 11 total and phosphorylated members of the Akt/mTOR signalling pathway (Akt^{Ser473}, $GSK3\alpha^{Ser21}$, $GSK3\beta^{Ser9}$, $IGF1R^{Tyr1135/1136}$, $IR^{Tyr1162/Tyr1163}$, $IRS1^{Ser312}$, $mTOR^{Ser2448}$, $p70S6K^{Thr412}$, $PTEN^{Ser380}$, $RPS6^{Ser235/Ser236}$ and $TSC2^{Ser939}$). Mean fluorescence intensity values of analytes were measured in a MAGPIX system (Luminex Corporation, Austin, TX, USA). The mean fluorescence intensity of a particular phosphorylated protein was normalized to the total protein, and this ratio was further normalized to values from the $MSTN^{+/+}$ group.

Hydroxyproline assay

The hydroxyproline content of muscles was measured using a colorimetric assay as previously described (Woessner, 1961; Mendias *et al.* 2006). Briefly, muscles were dried for several hours at 110°C, weighed immediately, and then hydrolysed in 500 μl of 6 M HCl for 6 h at 110°C. The hydrolysate was removed and neutralized with an equal volume of 6 M NaOH. Known amounts of L-hydroxyproline (Sigma, St Louis, MO, USA) were used to construct a standard curve. Samples were assayed in triplicate using a Spectramax M5 microplate reader at an absorbance of 560 nm.

Measurement of whole-muscle contractile and mechanical properties

Contractile properties of EDL and soleus muscles were evaluated as previously described (Segal & Faulkner, 1985; Mendias *et al.* 2006). Briefly a 4–0 silk suture was tied to the proximal and distal tendons of intact EDL and soleus muscles, immediately distal to the aponeuroses. Following suture placement, muscles were then removed from the animal and immediately placed in a bath that contained Krebs mammalian Ringer solution supplemented with 0.3 mM tubocurarine chloride and 11 mM glucose. The bath was maintained at 25°C and bubbled with a mixture of 95% O_2 and 5% CO_2 to maintain a pH of 7.4. The distal tendon of the muscle was tied to a dual-mode servomotor/force transducer (Aurora Scientific, Aurora,

ON, Canada) and the proximal tendon tied to a fixed hook. Using square-wave pulses delivered from platinum electrodes connected to a high-power current stimulator (Aurora Scientific), muscles were stimulated to contract. Custom-designed software (LabVIEW, National Instruments, Austin, TX, USA) controlled pulse properties and servomotor activity and recorded data from the force transducer at 20 kHz. The voltage of pulses was serially increased, and the muscle length was increased or decreased to provide the length (L_o) that resulted in maximal twitch force (P_t). Muscles were held at L_o and stimulated with pulse trains of 300 ms for EDL muscles and 900 ms for soleus muscles to generate isometric contractions. The stimulus frequency was increased until the P_o was achieved. To calculate sP_o, P_o was divided by the physiological cross-sectional area (PCSA), which was determined by dividing the muscle mass by the product of fibre length (L_f) and 1.056 g cm^{-3}, the density of mammalian skeletal muscle.

After measurement of active force production, the passive mechanical properties of muscles were measured. Muscles were shortened to a value that was 0.3L_f shorter than L_o, and subsequently stretched passively to a length that was 0.3L_f greater than L_o at a velocity of 1L_f s^{-1}. After completion of passive stretch measurements, the maximal isometric force was again measured to verify that no mechanical stretch-induced injury had occurred. Muscles were then removed from the bath, weighed and immediately prepared for histology.

Permeabilized fibre contractility

The contractility of permeabilized muscle fibres from the TA was measured as previously described (Mendias *et al.* 2011; Gumucio *et al.* 2014). Briefly, fibre bundles approximately 4–6 mm in length and 0.5–0.75 mm in diameter were dissected from the deep aspect of the

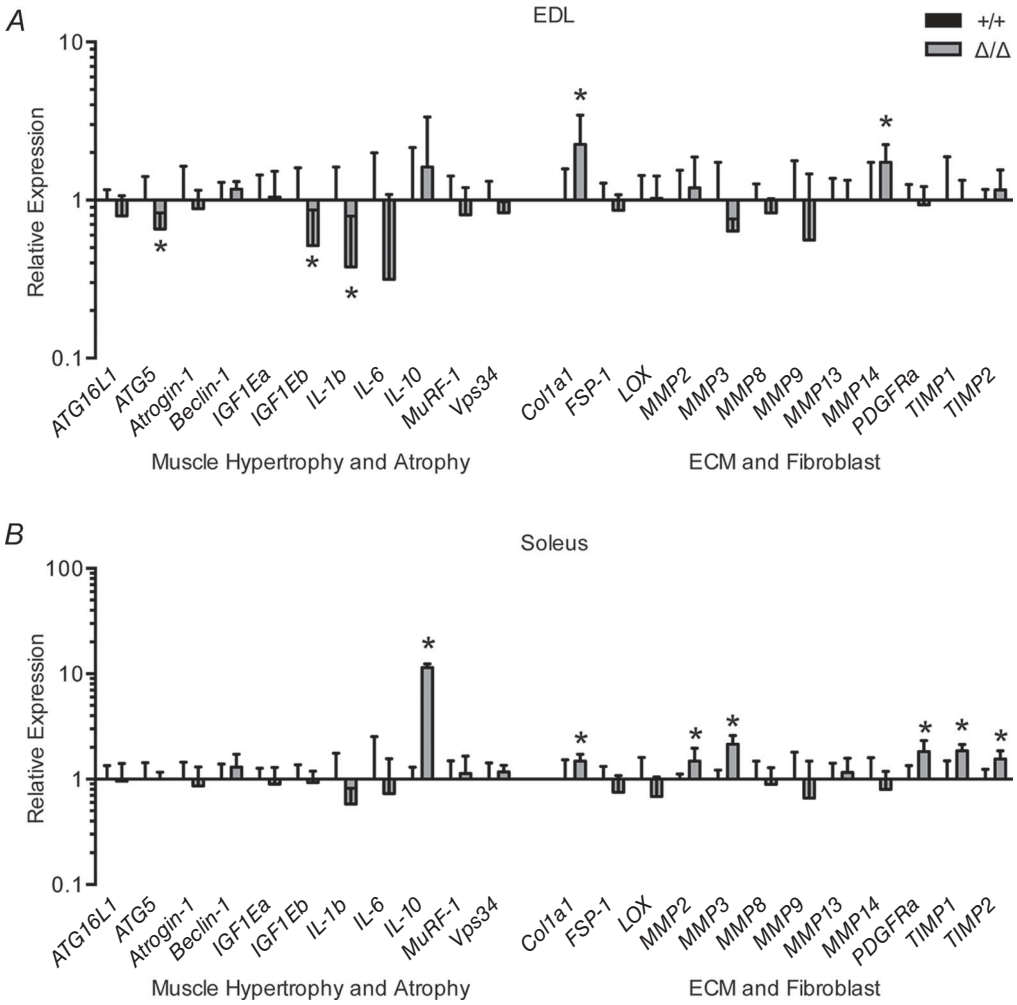

Figure 2. Messenger RNA expression from extensor digitorum longus (EDL; *A*) and soleus muscles (*B*)
Target genes are normalized to the stable housekeeping gene β-actin, and then further normalized to the *MSTN*$^{+/+}$ group.

muscle. Bundles were placed in skinning solution for 30 min and then in storage solution for 16 h at 4°C, followed by storage at −80°C. On the day of single-fibre testing, bundles were thawed slowly on ice, and individual fibres were pulled from bundles using fine mirror-finished forceps. Fibres were then placed in a chamber containing relaxing solution and secured at one end to a servomotor (Aurora Scientific) and at the other end to a force transducer (Aurora Scientific) using two ties of 10–0 monofilament nylon suture at each fibre end. The L_f was adjusted to obtain a sarcomere length of 2.5 μm using a laser diffraction measurement system. The average fibre CSA was calculated assuming an elliptical cross-section, with diameters obtained at five positions along the fibre from high-magnification images at two different views (top and side). The maximal fibre isometric force (F_o) was elicited by immersing the fibre in a solution containing a supra-physiological concentration of calcium. The specific force of fibres (sF_o) was calculated by dividing F_o by fibre CSA. Fibres were categorized as fast or slow by examining their force response to rapid, constant-velocity shortening, and 10 fast fibres were tested from each TA muscle from both groups.

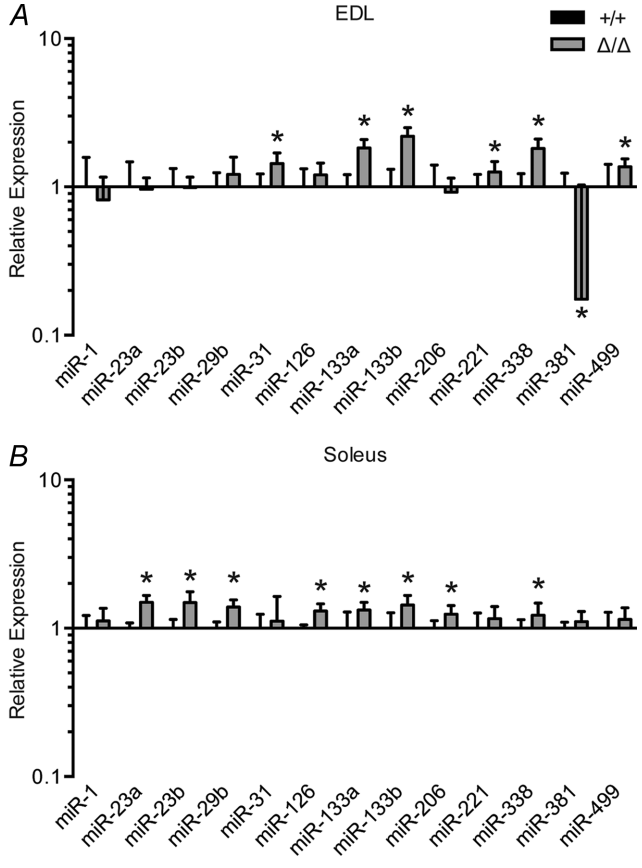

Figure 3. MicroRNA expression from EDL (*A*) and soleus muscles (*B*)
Target genes are normalized to the stable housekeeping gene *Rnu6*, and then further normalized to the *MSTN*$^{+/+}$ group.

Histology

Muscles and tendons were rinsed and snap frozen in Tissue-Tek (Sakura, Torrance, CA, USA) using isopentane cooled in liquid nitrogen, and stored at −80°C until use. Tissue was trimmed to obtain samples from the mid-belly, sectioned at a thickness of 10 μm in a cryostat and stained with Haematoxylin and Eosin or prepared for immunohistochemistry. Muscle fibre-type immunohistochemistry was performed as described previously (Gumucio *et al.* 2014). Briefly, sections were permeabilized in 0.2% Triton X-100 in PBS, blocked in 5% goat serum in PBS and incubated with monoclonal antibodies (Developmental Studies Hybridoma Bank, Iowa City, IA, USA) diluted 1:100 against type I myosin heavy chain (BA-D5, mIgG2b), type IIA myosin heavy chain (SC-71, mIgG1) and type IIB myosin heavy chain (BF-F3, mIgM). Primary antibodies were detected with highly cross-adsorbed, goat secondary antibodies that were conjugated to AlexaFluor probes and diluted 1:300 (Life Technologies, Grand Island, NY, USA). The absence of a fluorescence signal indicated type IIX fibres. Wheat germ agglutin lectin conjugated to AlexaFluor 488 (WGA-AF488; Life Technologies), diluted 1:200, was used to identify extracellular matrix. For plantaris tendons, sections were fixed with 4% paraformaldehyde and incubated with WGA-AF488 and with 4',6-diamidino-2-phenylindole (Sigma) to identify nuclei. Slides were imaged using a Zeiss Axiovert 200M microscope outfitted with the ApoTome system (Carl Zeiss, Thornwood, NY, USA). ImageJ software (NIH, Bethesda, MD, USA) was used to perform quantitative measurements.

Analysis of tendon mechanical properties

Plantaris muscle–tendon–bone units used for mechanical properties analysis were wrapped in saline-soaked gauze and stored at −20°C until use. Failure testing of plantaris tendons was performed as previously described (Mendias *et al.* 2008; Oak *et al.* 2014) using a modified ElectroForce ELF3200 uniaxial testing system (Bose, Eden Prairie, MN, USA) equipped with a 100 N load cell (Omega, Stamford, CT, USA). Plantaris tendons were removed from rats with their entheses and myotendinous junctions intact. Bone and muscle were secured tightly to vice grips and reinforced with ethyl cyanoacrylate. The tendon was pre-loaded to 1.0 N, and two cameras (JAI, San Jose, CA, USA) mounted 90 deg apart captured the front and side views of the tendon, which was then used to calculate tendon CSA by fitting width and length measurements to an ellipse, as well as the starting tendon length (L_o). The specimen was then stretched until failure at a rate of 10 mm s^{-1}, and the peak strain, peak stress, peak stiffness and energy absorption were determined from testing.

Statistical analysis

Data are presented as means ± SD. Differences between $MSTN^{+/+}$ and $MSTN^{\Delta/\Delta}$ groups were tested using Student's unpaired t tests ($\alpha = 0.05$). For growth curve data, the Holm–Sidak method was used to correct statistical significance to account for multiple observations. Prism 6.0 software (GraphPad Software, San Diego, CA, USA) was used for analysis.

Results

Deletion of the splice acceptor of exon 2 of myostatin resulted in an 86% reduction in circulating myostatin levels (Fig. 1*C*) and a grossly apparent increase in muscle mass (Fig. 1*D*–*G*). The overall body mass of $MSTN^{\Delta/\Delta}$ rats was ∼20% greater than that of $MSTN^{+/+}$ rats at all time points measured, and the general shape of the growth curves was similar between the two genotypes (Fig. 1*H*). No difference in heart mass was present (Fig. 1*I*), but $MSTN^{\Delta/\Delta}$ rats had a 42% increase in TA mass compared with control rats (Fig. 1*J*).

For gene expression in EDL, $MSTN^{\Delta/\Delta}$ rats had a 35% reduction in *ATG5* expression, a 48% reduction in *IGF1Eb* expression and a 62% decrease in *IL-1β* expression, but no other differences were observed for genes related to muscle hypertrophy and atrophy (Fig. 2*A*). Type I collagen expression was increased by 125% and *MMP-14* by 73% in $MSTN^{\Delta/\Delta}$ rats, but otherwise the expression of genes related to ECM synthesis or fibroblast makers was similar between the two groups (Fig. 2*A*). In EDL, expression of miR-31 was elevated in $MSTN^{\Delta/\Delta}$ rats by 43%, miR-133a by 83%, miR-133b by 120%, miR-221 by 26%, miR-338 by 82% and miR-499 by 36%, while miR-381 was downregulated by 83% (Fig. 3*A*). In soleus muscles of $MSTN^{\Delta/\Delta}$ rats, IL-10 expression elevated by 1046% over $MSTN^{+/+}$ rats, but no other changes in muscle hypertrophy and atrophy genes were noted (Fig. 2*B*). With

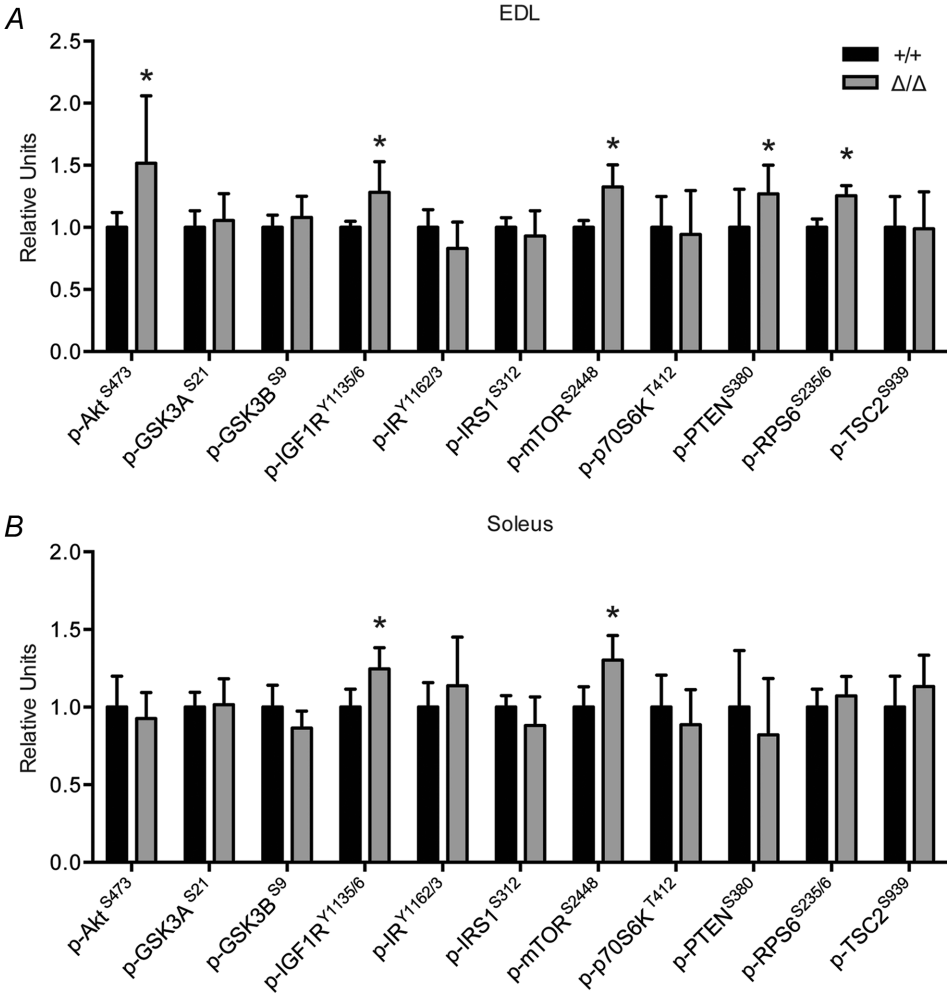

Figure 4. Abundance of phosphoproteins from EDL (*A*) and soleus muscles (*B*)
The abundance of specific phosphoproteins was normalized to the total protein abundance, and then further normalized to values from $MSTN^{+/+}$ rats.

ECM synthesis and fibroblast regulatory genes, expression in soleus of $MSTN^{\Delta/\Delta}$ rats was 47% greater for type I collagen and *MMP-2*, 114% greater for *MMP-3*, 82% greater for *PDGFRα*, 85% greater for *TIMP1* and 55% greater for *TIMP2*. For miRNAs in soleus, $MSTN^{\Delta/\Delta}$ rats had a 49% increase in miR-23a and miR-23b, a 39% increase in miR-29b, a 31% increase in miR-126 and miR-133a, a 43% increase in miR-133b and a 23% increase in miR-206 and miR-338 expression (Fig. 3*B*).

We then evaluated the relative content of various phosphoproteins and collagen in muscles. For the EDL (Fig. 4*A*), there were increases of 52% in p-Akt^{Ser473}, 28% in p-IGF1R$^{Tyr1135/1136}$, 33% in p-mTOR^{Ser2448}, 27% in p-PTEN^{Ser380} and 25% in RPS6$^{Ser235/Ser236}$ for $MSTN^{\Delta/\Delta}$ rats *vs.* $MSTN^{+/+}$ rats. No differences were observed in p-GSK3α^{Ser21}, p-GSK3β^{Ser9}, p-IR$^{Tyr1162/Tyr1163}$, p-IRS1^{Ser312}, p-p70S6K^{Thr412} or p-TSC2^{Ser939}. In soleus muscles (Fig. 4*B*), $MSTN^{\Delta/\Delta}$ rats had a 25% increase in p-IGF1R$^{Tyr1135/1136}$ and a 30% increase in p-mTOR^{Ser2448}, but no differences were observed in the levels of other phosphoproteins. For collagen content, no differences in hydroxyproline content were observed between $MSTN^{+/+}$ and $MSTN^{\Delta/\Delta}$ rats for EDL and soleus muscles (Fig. 5).

For muscle contractility measurements, at the level of the single muscle fibre, no differences in CSA, F_o or sF_o were observed (Fig. 6). For the EDL muscle, there was a 33% increase in mass, a 31% increase in PCSA, a 57% increase in P_o and no difference in sP_o production in $MSTN^{\Delta/\Delta}$ rats (Fig. 7*A–D*). No differences in muscle length or in passive mechanical properties were observed (Table 1), and fibres in both genotypes appeared grossly healthy (Fig. 8*A*). The $MSTN^{\Delta/\Delta}$ rats had a 37% increase in overall fibres per muscle, with an approximate 20% increase in the size of type IIA, IIB, IIX, IIA/IIX and IIB/IIX fibres (Fig. 8*C* and *D*). There was an overall 80% reduction in the proportion of type I fibres and a 26% reduction in type IIA/IIX fibres in $MSTN^{\Delta/\Delta}$ rats, with a 25% increase in the number of type IIB fibres (Fig. 8*E*). Soleus muscles of $MSTN^{\Delta/\Delta}$ rats demonstrated a 20% increase in mass, a 22% increase in PCSA, a 20% increase in P_o and no difference in sP_o compared with $MSTN^{+/+}$ rats (Fig. 7*E–H*). Soleus muscle lengths were similar between genotypes, but $MSTN^{\Delta/\Delta}$ rats had a 12% reduction in peak passive stress and a 14% reduction in passive energy absorption, with no differences in peak passive load or stiffness (Table 1). Overall fibre appearance was generally healthy (Fig. 8*A*). The $MSTN^{\Delta/\Delta}$ rats had a 45% increase in overall fibres per muscle (Fig. 8*F*). No change in fibre area was observed, but $MSTN^{\Delta/\Delta}$ rats had a 6% reduction in type I fibres (Fig. 8*G* and *H*).

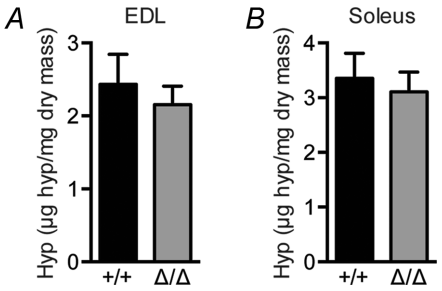

Figure 5. Hydroxyproline (hyp) content of EDL (*A*) and soleus muscles (*B*)
Total hydroxyproline was normalized to the dry mass of muscles.

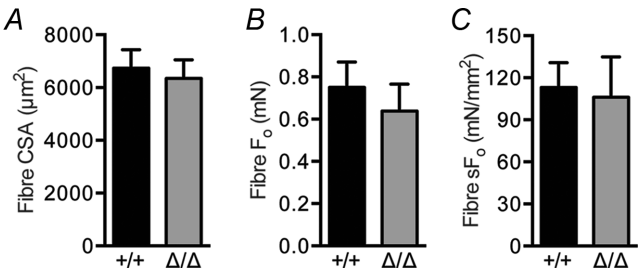

Figure 6. Contractility of permeabilized TA muscle fibres
A, muscle fibre cross-sectional area (CSA). *B*, maximal isometric force (F_o). *C*, specific maximal isometric force (sF_o).

After measuring muscle mechanics, morphology and biochemistry, we next determined the structure and function of tendons. No difference in absolute TA or plantaris tendon masses were observed, although the ratio of TA tendon to muscle mass was reduced by 26% in $MSTN^{\Delta/\Delta}$ rats (Fig. 9*A* and *B*). The overall CSA and cell density of plantaris tendons was similar between the two groups (Fig. 9*C* and *D*). Regarding the measurement of mechanical properties, the initial measurements of length and CSA were made when tendons were held at a length that produced 1 N of total load, which was just past the toe region of the stress-strain graph. No difference in L_o was observed, but the overall nominal CSA of tendons was reduced by 23% in $MSTN^{\Delta/\Delta}$ rats. Tendons were then stretched to yield, and although a 20% reduction in peak strain was observed, no differences in peak stress, peak stiffness or energy absorption during the stretch were observed (Fig. 10).

Finally, we measured the expression of several genes important in determining the composition and mechanical properties of tendon ECM, as well as genes involved in regulating tendon fibroblast activity. Compared with $MSTN^{+/+}$ rats, $MSTN^{\Delta/\Delta}$ rats had increases of 141% for *MMP-9*, 524% for *MMP-14*, 2112% for *Egr2* and 84% for *mohawk*, but otherwise no differences in gene expression were observed (Fig. 11).

Discussion

Myostatin has one of the greatest effects on skeletal muscle mass of any single signalling molecule, with genetic deficiencies of myostatin in mice resulting in gains of muscle mass of 50–100% or more (McPherron *et al.*

2006; Mendias *et al.* 2006; Lee, 2007; Gentry *et al.* 2011). In the present study, genetic inactivation of myostatin through the induction of a zinc finger nuclease-mediated frameshift mutation resulted in rats with marked increases in muscle mass. Although the gains in muscle mass of $MSTN^{\Delta/\Delta}$ rats compared with $MSTN^{+/+}$ rats was not quite as great as the extent previously reported in EDL and soleus muscles of mice (Mendias *et al.* 2006), the $MSTN^{\Delta/\Delta}$ rats had improvements in force production that were generally greater than those observed in mice. The dramatic stiffening of muscle and tendon ECM previously observed in myostatin-deficient mice (Mendias *et al.* 2006, 2008) did not occur in myostatin-deficient rats. The overall results from this study indicate that inactivation of myostatin in rats resulted in marked increases in muscle mass and improved force production without some of the detrimental effects on muscle and tendon contractile and mechanical properties observed in myostatin-deficient mice.

Myostatin appears to regulate muscle fibre size by interacting with both the protein synthesis and degradation pathways in muscle fibres. Atrogin-1 and MuRF-1, which are induced in response to myostatin, are among the chief E3 ubiquitin ligases expressed in skeletal muscle that direct the polyubiqutination of proteins to target them for proteolysis by the 26S proteasome (Lokireddy *et al.* 2011; Mendias *et al.* 2011; McFarlane *et al.* 2012). Autophagy is another important cellular process responsible for protein degradation in skeletal muscle, and myostatin signalling can activate this pathway and trigger the formation of autophagosomes (Lee *et al.* 2011). Myostatin also inhibits protein synthesis by blocking the IGF-1/PI3K/Akt pathway and subsequent activation of p70S6K (Yang *et al.* 2007; Amirouche *et al.* 2009; Trendelenburg *et al.* 2009). In the present study, no differences in atrogin-1 or MuRF-1 were observed between $MSTN^{+/+}$ and $MSTN^{\Delta/\Delta}$ rats in both EDL and soleus muscles. *ATG5*, which is important for phagophore elongation and maturation (Sandri, 2011), was downregulated in EDL muscles of $MSTN^{\Delta/\Delta}$ rats, but no differences in expression were present for other key regulators of autophagy, *ATG16L1*, *beclin-1* or *Vps34*. Interleukin-1β and interleukin-6 are atrophy-inducing cytokines, whose activity can be countered by interleukin-10 (Muñoz-Cánoves *et al.* 2013; Thompson *et al.* 2013). Interleukin-1β was downregulated in EDL muscles of $MSTN^{\Delta/\Delta}$ rats, while *IL-10* was markedly induced in soleus muscles of $MSTN^{\Delta/\Delta}$ rats. Several of the miRNAs involved in the adaptation of muscle to mechanical loading, termed myomiRs (Kirby & McCarthy, 2013), were differentially regulated by inactivation of myostatin. Reductions in miR-1 and miR-133a, which target IGF-1Ea and its receptor, are downregulated during hypertrophy in mice (McCarthy & Esser, 2006), but in the present study no differences in miR-1 were observed and miR-133a was elevated in both muscles from $MSTN^{\Delta/\Delta}$ rats. Although no difference in *IGF-1Ea* expression was observed, EDL and soleus muscles of $MSTN^{\Delta/\Delta}$ rats had increased levels of p-IGF-1 receptor and p-mTOR. Further activation of downstream components of the IGF-1 pathway in EDL muscles is supported by increased levels of p-PTEN, and although p-p70S6K levels were not different, the levels of the translation–regulation protein p-RPS6 were elevated in $MSTN^{\Delta/\Delta}$ rats.

While the results regarding components of the muscle hypertrophy pathway were anticipated, the minimal

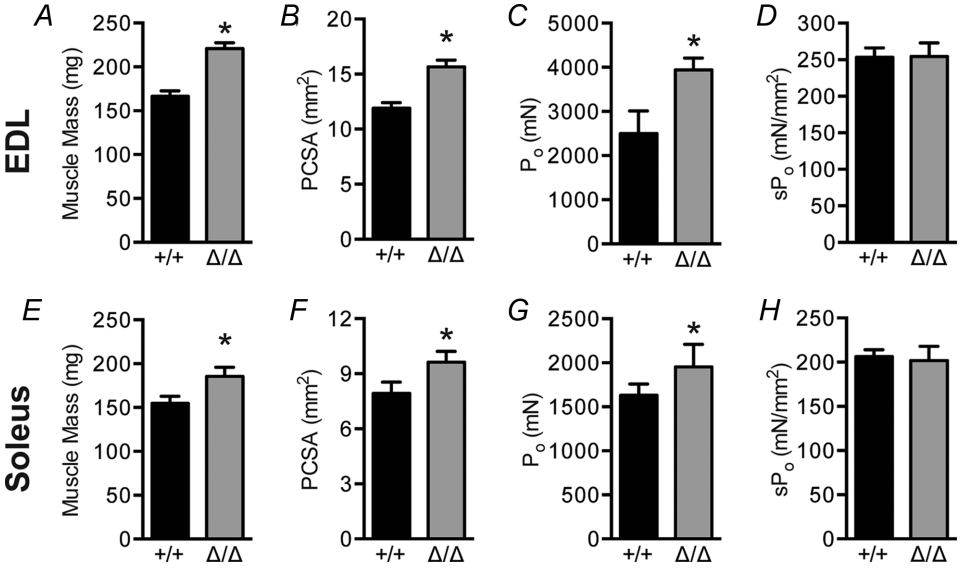

Figure 7. Mass and contractility of EDL (*A–D*) and soleus muscles (*E–H*)
A and *E*, whole muscle mass. *B* and *F*, physiological cross-sectional area (PCSA). *C* and *G*, maximal isometric force (P_o). *D* and *H*, specific maximal isometric force (sP_o).

Table 1. Twitch and passive mechanics measurements from extensor digitorum longus and soleus muscles of *MSTN*$^{+/+}$ and *MSTN*$^{\Delta/\Delta}$ rats

Parameter	*MSTN*$^{+/+}$	*MSTN*$^{\Delta/\Delta}$
Extensor digitorum longus		
Muscle mass (mg)	170.7 ± 7.6	224.6 ± 4.4*
L_o (mm)	33.8 ± 0.8	33.9 ± 1.3
L_f (mm)	13.5 ± 0.3	13.6 ± 0.5
Peak twitch force (mN)	928.1 ± 70.6	1235 ± 179*
Specific peak twitch force (mN mm^{-2})	78.0 ± 5.3	78.8 ± 9.5
Time-to-peak twitch tension (ms)	27.0 ± 0.7	27.5 ± 1.2
Half-relaxation time (ms)	21.2 ± 2.1	17.8 ± 1.2*
Maximal twitch dP/dt (mN ms^{-1})	62.5 ± 6.5	79.7 ± 20.1*
Peak passive load (mN)	588.7 ± 289.0	568.5 ± 341.0
Peak passive stress (mN mm^{-2})	49.9 ± 25.6	36.9 ± 23.4
Peak passive stiffness (mN mm^{-2})	499.6 ± 159.7	465.5 ± 200.9
Passive stretch energy absorption (mJ g^{-1})	4.2 ± 2.2	3.3 ± 2.0
Soleus		
Muscle mass (mg)	154.8 ± 8.0	185.5 ± 10.6*
L_o (mm)	31.4 ± 0.8	31.4 ± 1.4
L_f (mm)	18.8 ± 0.5	18.8 ± 0.8
Peak twitch force (mN)	377.2 ± 68.2	452.8 ± 65.4*
Specific peak twitch force (mN mm^{-2})	47.5 ± 7.5	47.0 ± 6.4
Time-to-peak twitch tension (ms)	89.3 ± 10.1	77.1 ± 5.0*
Half-relaxation time (ms)	164.5 ± 19.3	124.5 ± 14.7*
Maximal twitch dP/dt (mN ms^{-1})	11.1 ± 1.8	15.2 ± 2.6*
Peak passive load (mN)	2392.0 ± 248.9	2596 ± 448.2
Peak passive stress (mN mm^{-2})	301.7 ± 22.1	265.8 ± 35.0*
Peak passive stiffness (mN mm^{-2})	676.0 ± 175.2	789.6 ± 82.4
Passive stretch energy absorption (J kg^{-1})	32.5 ± 0.7	27.8 ± 5.6*

Abbreviations: dP/dt, rate of force development; L_f, fibre length; L_o, length that results in maximal twitch force; *MSTN*$^{+/+}$, wild-type control; and *MSTN*$^{\Delta/\Delta}$, myostatin knock-out. Values are means ± SD; $n = 6$ for *MSTN*$^{+/+}$ rats and $n = 7$ for *MSTN*$^{\Delta/\Delta}$ rats. Differences were tested with Student's unpaired t tests

*significantly different from *MSTN*$^{+/+}$ rats ($P < 0.05$).

involvement of atrophy genes was surprising. The discrepancies between the present findings and previously reported studies of myostatin are likely to be due to two factors. First, most of the studies on myostatin signalling have been conducted in cultured murine myotubes using high doses of myostatin, and it is possible that findings from this system are unique to the *in vitro* environment, where it is possible to control levels of growth factors and other media components tightly. Second, a species-specific difference in response to myostatin may be present. Even within the *in vitro* environment, murine myotubes robustly activate canonical atrophy pathways in response to myostatin, while human myotubes are far less responsive (Trendelenburg *et al.* 2009; Lokireddy *et al.* 2011; McFarlane *et al.* 2012). The results from the present study suggest that in rats, myostatin deficiency has little impact on atrophy-related genes *in vivo*, and this is in agreement with recent work that posited the role of myostatin signalling in muscle is to prevent activation of hypertrophy signalling pathways, not to induce muscle atrophy pathways directly (Sartori *et al.* 2013).

Most studies have indicated that blocking myostatin leads to an increase in P_o at the whole-muscle level, but sP_o has been reported either to decrease (Mendias *et al.* 2006; Matsakas *et al.* 2007; Schirwis *et al.* 2013) or not to change (Gentry *et al.* 2011; Murphy *et al.* 2011). Using *in vitro* measurements from 10- to 12-month-old mice, we found that compared with wild-type control animals the myostatin-deficient mice demonstrated a 63% increase in PCSA, a 34% increase in P_o and an 18% decrease in sP_o for the EDL, and a 30% increase in PCSA and P_o, with no change in sP_o for the soleus (Mendias *et al.* 2006). The reduction in sP_o for EDL muscles led us to study changes in contractility at the single-fibre level, which demonstrated that compared with wild-type mice, fibres from myostatin-deficient mice had an increase in CSA, no change in F_o and a subsequent reduction in sF_o (Mendias *et al.* 2011). These findings were supported by Qaisar *et al.* (2012), who also observed a decrease in sF_o in single fibres from myostatin-deficient mice.

We postulated that the reason EDL muscles from myostatin-deficient mice had greater mass and P_o at the

whole-muscle level was due to the dramatic 66% increase in the number of fibres present in their muscles (Mendias *et al.* 2006, 2011). Furthermore, the decrease in protein degradation in myostatin-deficient mice was likely to lead to a reduction in the ability to target proteins to the ubiquitin–proteasome system efficiently in normal homeostatic conditions, resulting in an accumulation of proteins that physically took up space but did not contribute to force production and a subsequent decrease in sP_o. This is supported by other studies, which have reported the presence of swollen fibres and inclusion body protein aggregates in the muscles of myostatin-deficient mice (Amthor *et al.* 2007; Gentry *et al.* 2011).

In the present study, at the whole-muscle level the $MSTN^{\Delta/\Delta}$ rats had an increase in PCSA and fibre abundance and, much to our surprise, had an increase in

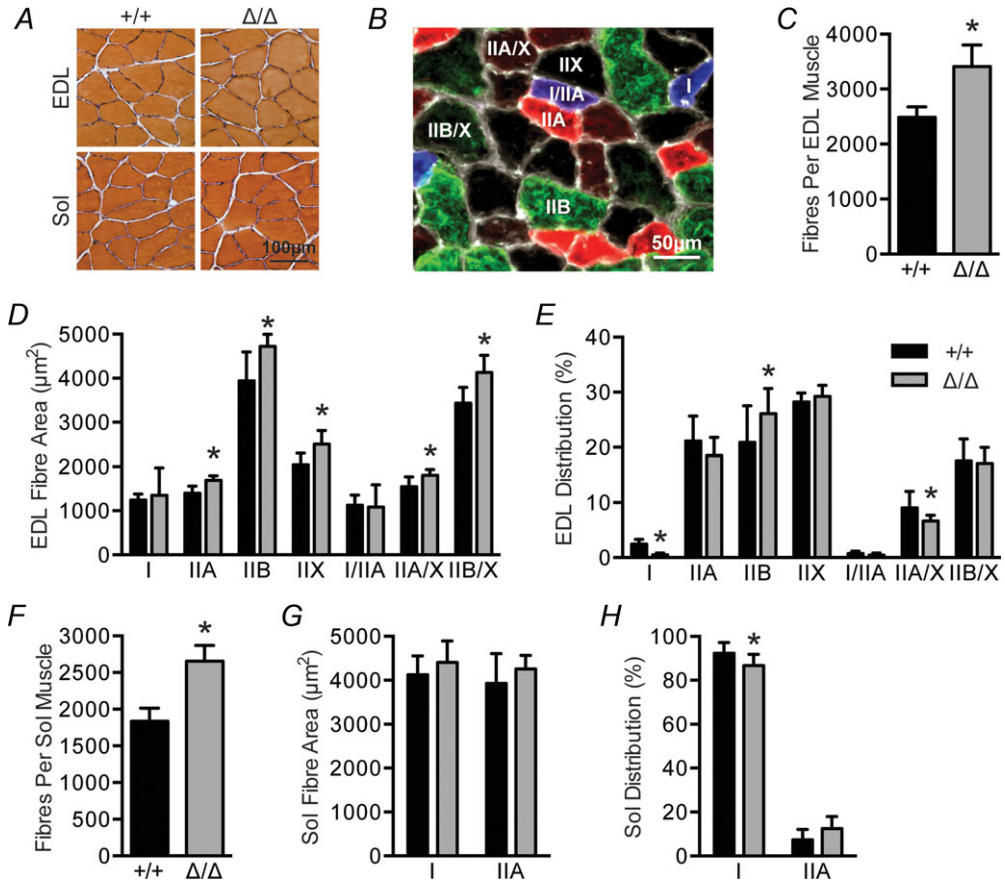

Figure 8. Fibre-type distribution and size of EDL (*B–E*) and soleus muscles (*F–H*)
A, representative images of Haematoxylin- and Eosin-stained sections from EDL and soleus muscles demonstrating the grossly healthy appearance of fibres. *B*, representative image from an EDL muscle demonstrating the different fibre types measured. *C* and *F*, fibres per muscle. *D* and *G*, size of fibres. *E* and *H*, distribution of fibres.

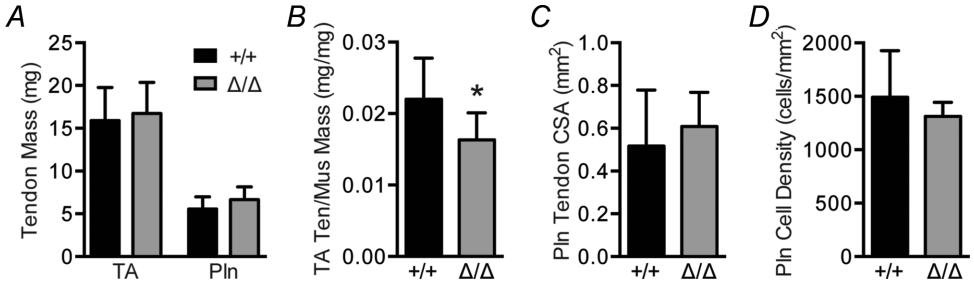

Figure 9. Tendon mass, size and cell density
A, mass of tibialis anterior (TA) and plantaris (Pln) tendons. *B*, TA tendon mass normalized to the mass of its muscle. Cross-sectional area (CSA; *C*) and cell density measurements (*D*) from full-thickness histological sections taken from the mid-belly of the tendon.

P_o without a reduction in sP_o and no differences in CSA, F_o or sF_o at the single-fibre level. No grossly apparent inclusion bodies, centrally located nuclei, swollen or ragged fibres or other pathological features were noted in muscle sections. The EDL muscles of $MSTN^{\Delta/\Delta}$ rats had modest increases in the CSA of many muscle fibre types, as well as a reduction in the percentage of type I fibres and an increase in type IIB fibres, which is consistent with observations in myostatin-deficient mice and cattle (Deveaux *et al.* 2001; Girgenrath *et al.* 2005; Gentry *et al.* 2011). No differences were present for soleus muscles, though. When combined, these results indicate that the genetic deficiency of myostatin in rats causes increased force production at the whole-muscle level chiefly through hyperplasia, with modest contributions from hypertrophy. Furthermore, the muscle appeared grossly healthy, without a decrease in sP_o and sF_o that was previously observed in some reports in mice, suggesting that the negative effects of myostatin inhibition on muscle contractility are not present in rats.

In addition to muscle fibres, myostatin appears to regulate the composition and mechanical properties of the muscle ECM, including tendons. Treatment of cultured mouse muscle cells, muscle fibroblasts or tendon fibroblast cells with myostatin induces the expression of type I collagen (Mendias *et al.* 2006, 2008; Li *et al.* 2008), and inhibition of myostatin in injured mice and in *mdx* mice reduced fibrosis (McCroskery *et al.* 1997; Wagner *et al.* 2002). The collagen content of myostatin-deficient mice is reduced by 73% in EDL muscles, with no differences observed for soleus muscles (Mendias *et al.* 2006). The collagen content of cattle with deficiencies in myostatin

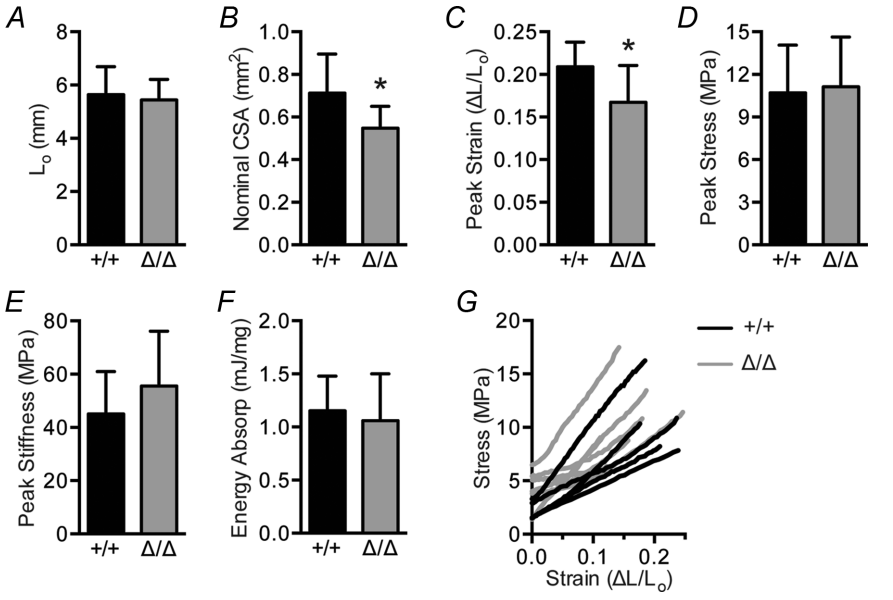

Figure 10. Mechanical properties of tendons tested until yield
A, starting tendon length (L_o). *B*, nominal CSA. *C*, peak strain to yield. *D*, peak stress to yield. *E*, peak stiffness to yield. *F*, energy absorption during the test. *G*, stress–strain graphs of samples.

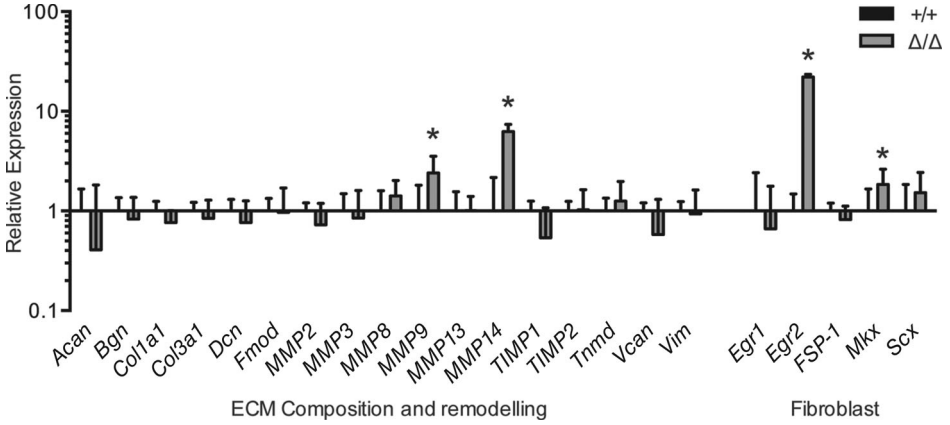

Figure 11. Messenger RNA expression from tendons
Target genes are normalized to the stable housekeeping gene β2-microglobulin, and then further normalized to the $MSTN^{+/+}$ group.

is either not different or modestly reduced depending on the muscle and the analysis technique (Ngapo *et al.* 2002; Raes *et al.* 2003).

In the present study, surprisingly we observed a mild increase in collagen expression in both EDL and soleus muscles of $MSTN^{\Delta/\Delta}$ rats, as well as an increase in *MMP-14* in EDL, and an increase in *MMP-2* and *MMP-9* in soleus muscles. Inhibitors of matrix metalloproteinases, *TIMP-1* and *TIMP-2*, as well as the fibroblast progenitor cell marker *PDGFRα* (Joe *et al.* 2010), were moderately upregulated in $MSTN^{\Delta/\Delta}$ soleus muscles. Several miRNAs associated with increased collagen expression, miR-31, miR-221 and miR-338 (Gumucio *et al.* 2013), were also upregulated in $MSTN^{\Delta/\Delta}$ muscles. However, despite modest increases in type I collagen expression, no differences in relative hydroxyproline content of muscles were observed. While we were surprised to see a mild induction in type I collagen expression with no differences in hydroxyproline content, the corresponding increase in *MMP* expression could indicate that the ECM of $MSTN^{\Delta/\Delta}$ rats is undergoing greater turnover and remodelling to accommodate the increased relative size and hyperplasia of $MSTN^{\Delta/\Delta}$ muscles.

Compared with wild-type control animals, the tendons of myostatin-deficient mice are 40% smaller, have a 45% reduction in fibroblast density and have marked reductions in the expression of type I collagen and the tendon cell proliferation and ECM production genes scleraxis and tenomodulin (Mendias *et al.* 2008). The tendons of these mice are also 14-fold stiffer and have a peak strain less than half that of wild-type mice (Mendias *et al.* 2008). Myostatin expression in tendons is downregulated in rats after unloading, and treatment of injured tendons with myostatin increased CSA but decreased peak stress of the tissue (Eliasson *et al.* 2009). Based on these findings, we anticipated that we would see dramatic stiffening and hypocellularity of tendons in $MSTN^{\Delta/\Delta}$ rats, but this was not observed. Although relative tendon mass was reduced, the absolute mass of tendons was not different between $MSTN^{+/+}$ and $MSTN^{\Delta/\Delta}$ rats. While no differences in tendon CSA were observed in histological measurements, nominal tendon CSA was reduced slightly when tendons were loaded to 1 N of force. No differences in peak stress were present, and although peak strain was reduced by about a fifth, a failure this high is far outside of the normal physiological ranges of strain in which tendons operate. For gene expression, no difference in type I collagen expression was observed, and modest elevations in *MMP-9* and *MMP-14* were present in $MSTN^{\Delta/\Delta}$ tendons. There were also no differences between $MSTN^{+/+}$ and $MSTN^{\Delta/\Delta}$ rats for the expression of genes related to fibroblast proliferation and remodelling, such as scleraxis or tenomodulin. This is in contrast to tendons from myostatin-deficient mice, which have marked reductions in type I collagen, scleraxis and tenomodulin (Mendias *et al.* 2008). Curiously, though, a robust 20-fold increase in the expression of *Egr2* was noted. Early growth response protein 2 (Egr2) is a member of the early growth response transcription factor family that is important in the differentiation and ECM production of tendon fibroblasts (Léjard *et al.* 2011). Expression of Egr2 is robustly induced in response to transforming growth factor-β signalling, but not activin signalling (Mazhawidza *et al.* 2005; Fang *et al.* 2011). It is possible that another member of the transforming growth factor-β superfamily which induces fibroblast cell proliferation and collagen synthesis, but does not signal through the activin receptors, is upregulated to compensate for the absence of signals from myostatin, resulting in the observed induction in *Egr2* and overall similar ECM composition and fibroblast gene expression patterns.

There are several limitations to this study. While the currently available genetic techniques are able to remove large regions of the genome in mice, the ability to manipulate the rat genome is more limited. As such, the mutation was targeted to the myostatin propeptide region to disrupt the proper folding and processing of myostatin. Although there is a small amount of myostatin remaining in circulation, because the propeptide is required for proper folding of myostatin, it is not clear whether the myostatin found in $MSTN^{\Delta/\Delta}$ rats has any biological activity. We evaluated only male rats at 6 months of age, and further studies looking at both sexes and different time points will no doubt be informative. Rats in this study lacked myostatin throughout their lifespan, and the observed hyperplasia in $MSTN^{\Delta/\Delta}$ muscles is likely to have occurred as a result of developmental mechanisms, with hyperplasia unlikely to occur if myostatin is inhibited postnatally. We did not evaluate changes in mechanical properties of the toe region of tendons and did not evaluate changes in hysteresis. Finally, while we measured the expression of several mRNAs, we did not quantify protein levels, and it is possible that changes in mRNA do not reflect changes in protein abundance. Despite these limitations, this work provided novel insight into changes in the structure and function of skeletal muscles and tendons in a large rodent model of myostatin deficiency.

As the inhibition of myostatin can result in substantial increases in total muscle mass and reductions in fibrosis, there has been much interest in the development of therapeutic inhibitors of myostatin for the treatment of a wide variety of muscle-wasting diseases (Gumucio & Mendias, 2012). Although there have been several encouraging preclinical studies in mouse models of diseases and injuries, the impaired contractile function and pathological changes to muscle fibres and their ECM in otherwise healthy mice has provided some pause with regard to the ability to implement therapies that target myostatin safely in patients. The nature of

myostatin inhibition in the present study is different from the pharmacological approaches that would occur therapeutically, but the pathological changes reported in some mouse models of myostatin deficiency did not occur in this rat model. Additionally, there has been concern about the potential abuse of myostatin inhibitors for doping purposes. However, no differences in force production were observed at the level of single fibres, and the overall increase in whole-muscle force production occurred mostly due to hyperplasia. While further studies are necessary, as hyperplasia does not occur in adult humans (Lexell, 1995), it is unlikely that blocking myostatin in otherwise healthy muscle fibres would result in noticeable improvements in muscle force production. For injuries or diseases that involve an upregulation in myostatin, therapeutic inhibition may still help to reduce muscle atrophy and lessen strength loss. Overall, the rat model of genetic deficiency of myostatin has provided important insight into species-specific changes in muscle and tendon morphology and mechanics and will be helpful in further basic and translational physiological studies.

References

Amirouche A, Durieux A-C, Banzet S, Koulmann N, Bonnefoy R, Mouret C, Bigard X, Peinnequin A & Freyssenet D (2009). Down-regulation of Akt/mammalian target of rapamycin signaling pathway in response to myostatin overexpression in skeletal muscle. *Endocrinology* **150**, 286–294.

Amthor H, Macharia R, Navarrete R, Schuelke M, Brown SC, Otto A, Voit T, Muntoni F, Vrbóva G, Partridge T, Zammit P, Bunger L & Patel K (2007). Lack of myostatin results in excessive muscle growth but impaired force generation. *Proc Natl Acad Sci USA* **104**, 1835–1840.

Castorena CM, Arias EB, Sharma N & Cartee GD (2014). Postexercise improvement in insulin-stimulated glucose uptake occurs concomitant with greater AS160 phosphorylation in muscle from normal and insulin-resistant rats. *Diabetes* **63**, 2297–2308.

Deveaux V, Cassar-Malek I & Picard B (2001). Comparison of contractile characteristics of muscle from Holstein and double-muscled Belgian Blue foetuses. *Comp Biochem Physiol A Mol Integr Physiol* **131**, 21–29.

Eliasson P, Andersson T, Kulas J, Seemann P & Aspenberg P (2009). Myostatin in tendon maintenance and repair. *Growth Factors* **27**, 247–254.

Eng CM, Smallwood LH, Rainiero MP, Lahey M, Ward SR & Lieber RL (2008). Scaling of muscle architecture and fiber types in the rat hindlimb. *J Exp Biol* **211**, 2336–2345.

Fang F, Ooka K, Bhattachyya S, Wei J, Wu M, Du P, Lin S, Del Galdo F, Feghali-Bostwick CA & Varga J (2011). The early growth response gene *Egr2* (alias Krox20) is a novel transcriptional target of transforming growth factor-β that is up-regulated in systemic sclerosis and mediates profibrotic responses. *Am J Pathol* **178**, 2077–2090.

Gentry BA, Ferreira JA, Phillips CL & Brown M (2011). Hindlimb skeletal muscle function in myostatin-deficient mice. *Muscle Nerve* **43**, 49–57.

Geurts AM, Cost GJ, Freyvert Y, Zeitler B, Miller JC, Choi VM, Jenkins SS, Wood A, Cui X, Meng X, Vincent A, Lam S, Michalkiewicz M, Schilling R, Foeckler J, Kalloway S, Weiler H, Ménoret S, Anegon I, Davis GD, Zhang L, Rebar EJ, Gregory PD, Urnov FD, Jacob HJ & Buelow R (2009). Knockout rats via embryo microinjection of zinc-finger nucleases. *Science* **325**, 433.

Girgenrath S, Song K & Whittemore L-A (2005). Loss of myostatin expression alters fiber-type distribution and expression of myosin heavy chain isoforms in slow- and fast-type skeletal muscle. *Muscle Nerve* **31**, 34–40.

Gumucio JP, Davis ME, Bradley JR, Stafford PL, Schiffman CJ, Lynch EB, Claflin DR, Bedi A & Mendias CL (2012). Rotator cuff tear reduces muscle fiber specific force production and induces macrophage accumulation and autophagy. *J Orthop Res* **30**, 1963–1970.

Gumucio JP, Korn MA, Saripalli AL, Flood MD, Phan AC, Roche SM, Lynch EB, Claflin DR, Bedi A & Mendias CL (2014). Aging-associated exacerbation in fatty degeneration and infiltration after rotator cuff tear. *J Shoulder Elbow Surg* **23**, 99–108.

Gumucio JP & Mendias CL (2013). Atrogin-1, MuRF-1, and sarcopenia. *Endocrine* **43**, 12–21.

Heinemeier KM, Olesen JL, Schjerling P, Haddad F, Langberg H, Baldwin KM & Kjaer M (2007). Short-term strength training and the expression of myostatin and IGF-I isoforms in rat muscle and tendon: differential effects of specific contraction types. *J Appl Physiol* **102**, 573–581.

Jiang M-S, Liang L-F, Wang S, Ratovitski T, Holmstrom J, Barker C & Stotish R (2004). Characterization and identification of the inhibitory domain of GDF-8 propeptide. *Biochem Biophys Res Commun* **315**, 525–531.

Joe AWB, Yi L, Natarajan A, LeGrand F, So L, Wang J, Rudnicki MA & Rossi FMV (2010). Muscle injury activates resident fibro/adipogenic progenitors that facilitate myogenesis. *Nat Cell Biol* **12**, 153–163.

Kirby TJ & McCarthy JJ (2013). MicroRNAs in skeletal muscle biology and exercise adaptation. *Free Radic Biol Med* **64**, 95–105.

Lee JY, Hopkinson NS & Kemp PR (2011). Myostatin induces autophagy in skeletal muscle *in vitro*. *Biochem Biophys Res Commun* **415**, 632–636.

Lee S-J (2004). Regulation of muscle mass by myostatin. *Annu Rev Cell Dev Biol* **20**, 61–86.

Lee S-J (2007). Quadrupling muscle mass in mice by targeting TGF-ss signaling pathways. *PLoS ONE* **2**, e789.

Lexell J (1995). Human aging, muscle mass, and fiber type composition. *J Gerontol A Biol Sci Med Sci* **50** Spec No., 11–16.

Léjard V, Blais F, Guerquin M-J, Bonnet A, Bonnin M-A, Havis E, Malbouyres M, Bidaud CB, Maro G, Gilardi-Hebenstreit P, Rossert J, Ruggiero F & Duprez D (2011). EGR1 and EGR2 involvement in vertebrate tendon differentiation. *J Biol Chem* **286**, 5855–5867.

Li ZB, Kollias HD & Wagner KR (2008). Myostatin directly regulates skeletal muscle fibrosis. *J Biol Chem* **283**, 19371–19378.

Lokireddy S, McFarlane C, Ge X, Zhang H, Sze SK, Sharma M & Kambadur R (2011). Myostatin induces degradation of sarcomeric proteins through a Smad3 signaling mechanism during skeletal muscle wasting. *Mol Endocrinol* **25**, 1936–1949.

McCarthy JJ & Esser KA (2007). MicroRNA-1 and microRNA-133a expression are decreased during skeletal muscle hypertrophy. *J Appl Physiol* **102**, 306–313.

McCroskery S, Thomas M, Platt L, Hennebry A, Nishimura T, McLeay L, Sharma M & Kambadur R (2005). Improved muscle healing through enhanced regeneration and reduced fibrosis in myostatin-null mice. *J Cell Sci* **118**, 3531–3541.

McFarlane C, Plummer E, Thomas M, Hennebry A, Ashby M, Ling N, Smith H, Sharma M & Kambadur R (2006). Myostatin induces cachexia by activating the ubiquitin proteolytic system through an NF-κB-independent, FoxO1-dependent mechanism. *J Cell Physiol* **209**, 501–514.

McPherron AC, Lawler AM & Lee SJ (1997). Regulation of skeletal muscle mass in mice by a new TGF-β superfamily member. *Nature* **387**, 83–90.

Matsakas A, Macharia R, Otto A, Elashry MI, Mouisel E, Romanello V, Sartori R, Amthor H, Sandri M, Narkar V & Patel K (2012). Exercise training attenuates the hypermuscular phenotype and restores skeletal muscle function in the myostatin null mouse. *Exp Physiol* **97**, 125–140.

Mazhawidza W, Winters SJ, Kaiser UB & Kakar SS (2006). Identification of gene networks modulated by activin in LβT2 cells using DNA microarray analysis. *Histol Histopathol* **21**, 167–178.

Mendias CL, Bakhurin KI & Faulkner JA (2008). Tendons of myostatin-deficient mice are small, brittle, and hypocellular. *Proc Natl Acad Sci USA* **105**, 388–393.

Mendias CL, Gumucio JP & Lynch EB (2012). Mechanical loading and TGF-β change the expression of multiple miRNAs in tendon fibroblasts. *J Appl Physiol* **113**, 56–62.

Mendias CL, Kayupov E, Bradley JR, Brooks SV & Claflin DR (2011). Decreased specific force and power production of muscle fibers from myostatin-deficient mice are associated with a suppression of protein degradation. *J Appl Physiol* **111**, 185–191.

Mendias CL, Marcin JE, Calerdon DR & Faulkner JA (2006). Contractile properties of EDL and soleus muscles of myostatin-deficient mice. *J Appl Physiol* **101**, 898–905.

Muñoz-Cánoves P, Scheele C, Pedersen BK & Serrano AL (2013). Interleukin-6 myokine signaling in skeletal muscle: a double-edged sword? *FEBS J* **280**, 4131–4148.

Murphy KT, Chee A, Gleeson BG, Naim T, Swiderski K, Koopman R & Lynch GS (2011). Antibody-directed myostatin inhibition enhances muscle mass and function in tumor-bearing mice. *Am J Physiol Regul Integr Comp Physiol* **301**, R716–R726.

Ngapo TM, Berge P, Culioli J, Dransfield E, DeSmet S & Claeys E (2002). Perimysial collagen crosslinking and meat tenderness in Belgian Blue double-muscled cattle. *Meat Sci* **61**, 91–102.

Oak NR, Gumucio JP, Flood MD, Saripalli AL, Davis ME, Harning JA, Lynch EB, Roche SM, Bedi A & Mendias CL (2014). Inhibition of 5-LOX, COX-1, and COX-2 increases tendon healing and reduces muscle fibrosis and lipid accumulation after rotator cuff repair. *Am J Sports Med* **42**, 2860–2868.

Qaisar R, Renaud G, Morine K, Barton ER, Sweeney HL & Larsson L (2012). Is functional hypertrophy and specific force coupled with the addition of myonuclei at the single muscle fiber level? *FASEB J* **26**, 1077–1085.

Raes K, Balcaen A, Dirinck P, DeWinne A, Claeys E, Demeyer D & DeSmet S (2003). Meat quality, fatty acid composition and flavour analysis in Belgian retail beef. *Meat Sci* **65**, 1237–1246.

Sandri M (2011). New findings of lysosomal proteolysis in skeletal muscle. *Curr Opin Clin Nutr Metab Care* **14**, 223–229.

Sartori R, Schirwis E, Blaauw B, Bortolanza S, Zhao J, Enzo E, Stantzou A, Mouisel E, Toniolo L, Ferry A, Stricker S, Goldberg AL, Dupont S, Piccolo S, Amthor H & Sandri M (2013). BMP signaling controls muscle mass. *Nat Genet* **45**, 1309–1318.

Schirwis E, Agbulut O, Vadrot N, Mouisel E, Hourdé C, Bonnieu A, Butler-Browne G, Amthor H & Ferry A (2013). The beneficial effect of myostatin deficiency on maximal muscle force and power is attenuated with age. *Exp Gerontol* **48**, 183–190.

Schmittgen TD & Livak KJ (2008). Analyzing real-time PCR data by the comparative C(T) method. *Nat Protoc* **3**, 1101–1108.

Segal SS & Faulkner JA (1985). Temperature-dependent physiological stability of rat skeletal muscle in vitro. *Am J Physiol Cell Physiol* **248**, C265–C270.

Sharma N, Castorena CM & Cartee GD (2012). Tissue-specific responses of IGF-1/insulin and mTOR signaling in calorie restricted rats. *PLoS ONE* **7**, e38835.

Stinckens A, Georges M & Buys N (2011). Mutations in the myostatin gene leading to hypermuscularity in mammals: indications for a similar mechanism in fish? *Anim Genet* **42**, 229–234.

Thompson CD, Zurko JC, Hanna BF, Hellenbrand DJ & Hanna A (2013). The therapeutic role of interleukin-10 after spinal cord injury. *J Neurotrauma* **30**, 1311–1324.

Trendelenburg AU, Meyer A, Rohner D, Boyle J, Hatakeyama S & Glass DJ (2009). Myostatin reduces Akt/TORC1/p70S6K signaling, inhibiting myoblast differentiation and myotube size. *Am J Physiol Cell Physiol* **296**, C1258–C1270.

Wagner KR, McPherron AC, Winik N & Lee S-J (2002). Loss of myostatin attenuates severity of muscular dystrophy in *mdx* mice. *Ann Neurol* **52**, 832–836.

Woessner JF (1961). The determination of hydroxyproline in tissue and protein samples containing small proportions of this imino acid. *Arch Biochem Biophys* **93**, 440–447.

Yang W, Zhang Y, Li Y, Wu Z & Zhu D (2007). Myostatin induces cyclin D1 degradation to cause cell cycle arrest through a phosphatidylinositol 3-kinase/AKT/GSK-3β pathway and is antagonized by insulin-like growth factor 1. *J Biol Chem* **282**, 3799–3808.

Zimmers TA, Davies MV, Koniaris LG, Haynes P, Esquela AF, Tomkinson KN, McPherron AC, Wolfman NM & Lee S-J (2002). Induction of cachexia in mice by systemically administered myostatin. *Science* **296**, 1486–1488.

Additional information

Competing interests

None declared.

Author contributions

C.L.M., E.B.L. and J.P.G. designed the study, conducted experiments, analysed data and wrote the manuscript. M.D.F., D.S.R., D.W.V.P., S.M.R. and C.S.D. performed experiments and analysed data. All authors read and approved the final manuscript.

Funding

This work was supported by NIH grants R01-AR063649, F31-AR06593, T32-GM008322 and RC2-HL101681.

Authors' present addresses

E. B. Lynch: University of Kentucky, Lexington, KY, USA.

M. D. Flood: Department of Physiology, University of Arizona, Tucson, AZ, USA.